Indian Journal of Chemistry
Vol. 56A, October 2017, pp. 1021-1027

Preparation, characterization and photocatalytic activity of silicon and sulfur codoped mesoporous titanium dioxide photocatalyst

Zhongliang Shi, Xu Wang & Shuhua Yao*

School of Applied Chemistry, Shenyang University of Chemical Technology, Shenyang 110142, China

Email: ysh1997@163.com

Received 24 May 2017; revised and accepted 28 September 2017

A series of mesoporous titanium dioxide ($MTiO_2$) photocatalysts codoped with silicon and sulfur has been prepared by a template method using tetraethyl orthosilicate, thiourea and tetrabutyl titanate ($Ti(OC_4H_9)_4$) as precursors and Pluronic P123 as template. The photoabsorbance of the prepared photocatalysts has been measured by UV-vis diffusive reflectance spectroscopy and its microstructure characterized using scanning electron microscopy, diffraction (XRD) and N_2 adsorption-desorption measurements. The microcrystal of the codoped photocatalyst consistest of anatase phase and is present in the form of almost spherical particle. The photocatalytic activity has been studied by photodegradation of methyl blue in aqueous solution under UV and visible light irradiation. The results show that the amount of dopants, silicon and sulfur, influence the photoactivity. The photocatalyst codoped with 1 mol% silicon and 2 mol% sulfur exhibites the highest photoactivity. The synergistic effect of silicon and sulfur codoping in improves the photocatalytic activity considerably.

Keywords: Photocatalysts activity, Mesoporous materials, Titanium dioxide, Silicon, Sulfur, Codoping, Doped catalyst

Titanium dioxide (TiO_2), an inexpensive, non-toxic and biocompatible material, has been widely used in solar cells,[1] lithium-ion cells[2] and many others, and is a promising photocatalyst for remediation of organic pollutants in air[3, 4] and water.[5–8] Compared with TiO_2, mesoporous TiO_2 has attracted more widespread interests in different frontier areas of science owing to its distinctive properties like high surface area, uniform pore size distribution, and well-defined pore topology.[9] Convenient syntheses through different chemical routes, large diversity of framework structures and novel properties have made it an extremely active area of research. The unique feature for the synthesis of mesoporous TiO_2 is the use of supramolecular assembly of surfactant molecules as structure-directing agents such as dendrimers, polymers,[18] aromatic acid, *etc*. [10-15] Mesoporous TiO_2 has been prepared using various synthetic strategies, including the soft-templating pathway, e.g., surfactant micelles as templates[16,17] and hard templating.[18] In the recent years, mesoporous TiO_2 has been applied extensively in photocatalytic,[19-22] sensing,[23] and optoelectronic applications.[24,25] However, the major drawback, i. e., high band gap (*ca.* 3.0 eV for rutile and 3.2 eV for anatase), often restricted use of mesoporous TiO_2 for suitable applications. Mesoporous TiO_2 can be activated only by ultraviolet (UV) light because of its high energy band gap, so it is necessary to develop a novel photocatalyst, which shows a high activity under visible light irradiation. Thus, exploring visible light absorption and large surface areas of mesoporous TiO_2 is significant. An efficient process that shifts the optical response of active mesoporous TiO_2 from the UV to the visible spectral range and to longer wavelength is doping elements, which can provide a framework to more easily incorporate the photocatalytic and solar efficiency of this material.[26-28] At present, the investigations about doping elements is focused mainly on transition metal ions doping [29-31] and rare earth metal doping.[32-24] However, metal doping has several drawbacks such as thermal instability and the metal centers act as electron traps, which reduces the photocatalytic efficiency.

Asahi *et al.*[26] first reported the N-doped TiO_2 exhibiting photoabsorption at wavelengths longer than 400 nm and photocatalytic activity under visible light. From there on, some researchers paid much attention to the modification of titanium dioxide by incorporating nonmetals, such as phosphorous,[35] sulfur,[36] fluorine,[37] boron,[38] carbon.[39] Furthermore, there were a few reports on titanium dioxide photocatalysts codoped by two kinds of nonmetals.[40, 41] Obviously, doping with these nonmetals can decrease the band gap and result in the response to the visible

light of photocatalysts. To the best of our knowledge, codoping of silicon and sulfur in mesoporous TiO_2 and its application to photocatalytic oxidation of methylene blue in aqueous solution have not been reported so far. In the present study, we used Pluronic P123 as template, and tetrabutyl titanate, tetraethyl orthosilicate and thiourea as the sources of titanium, silicon and sulfur to prepare a series of mesoporous TiO_2 photocatalysts codoped with silicon and sulfur. Then, we focused on the characterization of the prepared mesoporous TiO_2 samples and investigation on the effect of codoping of silicon and sulfur on the photocatalytic activity of mesoporous TiO_2. The synergistic effect of two dopants that leads to the enhancement of photocatalytic activity is also discussed.

Materials and Methods

All the chemicals used in the study are of analytical grade. All the solutions in the study were prepared using de-ionized water. All glassware was cleaned by rinsing with hydroxylamine hydrochloride, soaking in 10% HCl, and rinsing with deionized water.

Synthesis procedure

In a typical synthesis, 0.01 mol (3.4 g) of tetrabutyltitanate ($Ti(OC_4H_9)_4$) was added to a solution containing 1.0 g of Pluronic P123 ($EO_{20}PO_{70}EO_{20}$) and 8.0 mL of anhydrous ethanol to obtain solution A. Tetraethyl orthosilicate, and thiourea was dissolved in the mixture of 2.0 mL of deionized water, 1.5 mL of glacial acetic acid and 8.0 mL of anhydrous ethanol at room temperature to get solution B. Then solution A was added drop-wise into solution B within 60 min through a separating funnel while keeping the reaction mixture vigorously magnetically stirred (200 r/min). The resulting white slurry was stirred continuously for 1 h, aged for 48 h at ambient temperature of *ca*. 20 °C, and dried for 10 h at 100 °C under reduced pressure to get the xerogel, which was crushed to a fine powder and further calcined at 500 °C for 2 h to remove the residual organic compounds resulting from the hydrolysis of the $Ti(OC_4H_9)_4$ and the surfactant to prepare the codoped photocatalyst. The calcined samples were labeled as Si_xS_y-$MTiO_2$, where *x* and *y* corresponded to the initial mole ratios of Si to Ti and S to Ti, respectively.

Characterization of photocatalysts

Scanning electron microscopy (SEM) microimages of the prepared samples were obtained on a Philips XL-30 (25 kV, LaB6 filament) scanning electron microscope. Wide-angle X-ray powder diffraction (XRD) patterns of all samples were obtained at room temperature with a Rigaku D/max-r B X-ray diffractometer using Cu Kα radiation, operated at 45 kV and 40 mA. Specific surface area and pore volume of samples was calculated using the BET method[42] from nitrogen adsorption-desorption isotherms measured at 77 K with a Micromeritics 2000 instrument (ASAP 2000, Micromeritics, USA). UV-vis absorption spectroscopy measurements were made with a UV-vis diffuse reflectance spectrophotometer (Shimadzu UV-2550). Reflectance spectra were referenced to $BaSO_4$.

Photocatalytic degradation studies

Methylene blue (MB), a representative dye, was chosen as a model pollutant and the degradation of MB (20 mg/L) was used to value the photocatalytic performance of the obtained samples under UV and visible light irradiation.

For the UV light experiments, studies were carried out using a magnetically stirred quartz reactor and an ultraviolet mercury lamp (150 W, 365 nm) at ambient temperature of *ca*. 20 °C. Sixty minute adsorption time in dark condition was allowed before the start of photoreactions. Then samples of the suspension were withdrawn after a definite time interval and filtered through 0.22 μm filter paper. The filtrates were analyzed for residual MB concentration using a UV-vis spectrophotometer (UV762, Shanghai Analysis Co.). For comparison, the pure mesoporous TiO_2 and single doped mesoporous TiO_2 were used as reference systems. All the experiments were carried out in triplicate. The results presented herein are the mean values with a total error of less than 5%.

The experiments with visible light irradiation were performed at ambient temperature of *ca*. 20 °C with a 150 W metal halide lamp as the light source. To limit the irradiation wavelength, the light beam was passed through a 410 nm cut filter (L41) to assure cut-off wavelengths shorter than 410 nm. Then, samples of the suspension were withdrawn after a definite time interval and filtered through 0.22 μm filter paper to analyze the residual MB concentration.

Results and Discussion

SEM analysis

SEM images of the pure $MTiO_2$ and $Si_{0.01}S_{0.02}$-$MTiO_2$ shows that particles of pure $MTiO_2$ congregated together so densely that few gaps existed between the

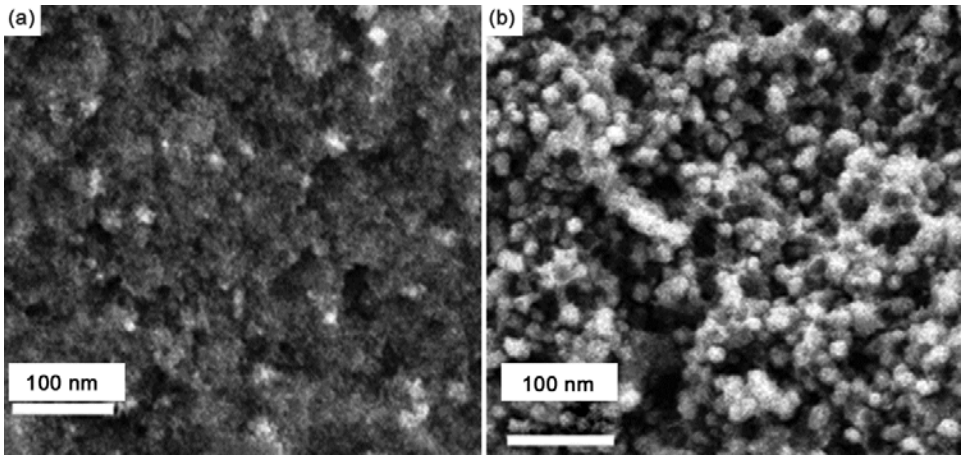

Fig. 1 — SEM images of $MTiO_2$ and Si-S codoped TiO_2; samples. [(a) $MTiO_2$; (b) $Si_{0.01}S_{0.02}$-$MTiO_2$].

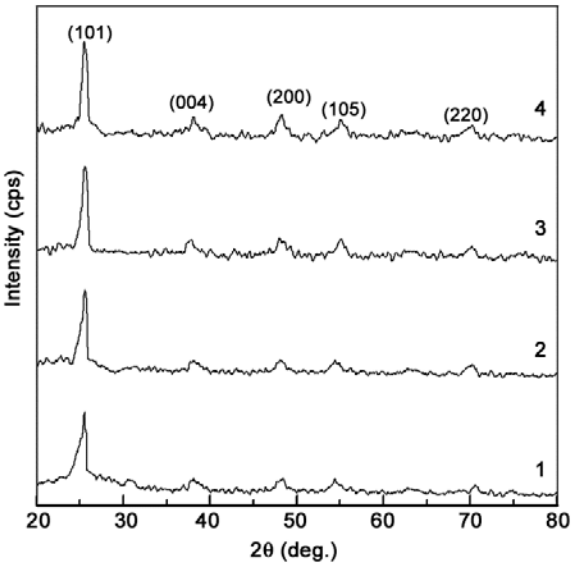

Fig. 2 — XRD patterns of $MTiO_2$ and Si-S codoped $MTiO_2$ samples. [$MTiO_2$ (1); $Si_{0.01}$-$MTiO_2$ (2); $S_{0.02}$-$MTiO_2$ (3); $Si_{0.01}S_{0.02}$-$MTiO_2$ (4)].

Table 1 — XRD analysis result of different TiO_2 samples

Sample	Crystallite size (nm)	Lattice parameters		
		a (nm)	*c* (nm)	*V* (nm^3)
$MTiO_2$	15.9	0.3786	0.9527	0.1366
$Si_{0.01}$-$MTiO_2$	17.5	0.3789	0.9522	0.1367
$S_{0.02}$-$MTiO_2$	16.9	0.3783	0.9515	0.1362
$Si_{0.01}S_{0.02}$-$MTiO_2$	18.2	0.3792	0.9518	0.1369

pores (Fig. 1). In contrast, the particles of codoped sample congregated loosely. It could be observed that all samples were present in the form of almost spherical particle with the average size of ~30 nm. This is in accordance with the values determined by XRD (20-30 nm).

XRD analysis

X-ray diffraction patterns were measured to obtain information on the crystal structure of the prepared photocatalysts. The XRD patterns of the prepared samples are shown in Fig. 2. It can be observed that all $MTiO_2$ powders were present in the anatase phases and that there was no evident difference between $MTiO_2$ and Si, S codoped $MTiO_2$. The diffraction peaks at 25.38°, 37.80°, 48.05°, 55.07° and 70.25° are consistent with the (101), (004), (200), (105) and (220) peaks of anatase titanium dioxide. The XRD results suggest that the Si and S codoping has little influence on the nature of crystal formation. The physical properties determined from XRD data of the samples are listed in Table 1. The average particle size of the prepared samples was ~15-20 nm. Compared with pure $MTiO_2$ ($a = b = 0.3786$ nm and $c = 0.9527$ nm), the lattice parameters *a* and *b* of the doped samples remained almost unvaried while the *c* parameters decreased. This demonstrates that the crystal lattices of the prepared samples were locally distorted by doping.

Nitrogen adsorption-desorption analysis

Information about BET specific surface area and pore volume of the prepared photocatalysts are summarized in Table 2. Measured BET surface areas of all samples had high surface area (160–180 $m^2\ g^{-1}$), the $Si_{0.01}S_{0.02}$-$MTiO_2$ displayed the highest specific surface area (179 $m^2\ g^{-1}$) and the highest pore volume (0.385 $cm^3\ g^{-1}$). The N_2 adsorption-desorption isotherms and Barret-Joyner-Halenda (BJH) pore size distribution plots (calculated from the adsorption branch) of $MTiO_2$ and $Si_{0.01}S_{0.02}$-$MTiO_2$ are shown in Fig. 3. The adsorption-desorption isotherms of all samples are of type IV with H2 hysteresis loop[43] with stepwise adsorption and desorption. The sharp decline

Table 2 — Physicochemical properties of $MTiO_2$ and Si-S codoped $MTiO_2$ samples

Sample	S_{BET} (m^2 g^{-1})	Total pore vol. (cm^3 g^{-1})	Avg. pore dia. (nm)	Eg (eV)
$MTiO_2$	161	0.372	10.3	3.22
$Si_{0.01}$-$MTiO_2$	166	0.376	9.8	3.11
$S_{0.02}$-$MTiO_2$	169	0.377	9.5	3.06
$Si_{0.01}S_{0.02}$-$MTiO_2$	179	0.385	9.4	2.96

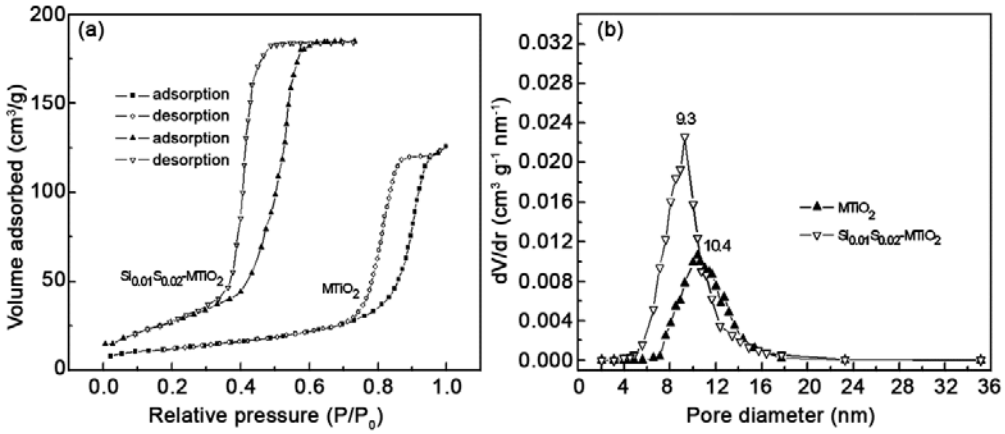

Fig. 3 — (a) N_2 adsorption-desorption isotherms of $MTiO_2$ and $Si_{0.01}S_{0.02}$-$MTiO_2$, and, (b) BJH pore size distributions of $MTiO_2$ and $Si_{0.01}S_{0.02}$-$MTiO_2$.

in the desorption curve and the hysteresis loop at high relative pressure are indicative of mesoporosity. During the process of adsorption, single molecular layer adsorption occurred at relatively low pressure and then multi-molecular layer adsorption occurred at higher pressure. The larger the sample pore sizes, the higher is the pressure of capillary cohesion.[44] As shown in Fig. 3, the capillary cohesion of $MTiO_2$ occurred at the higher pressure and that of $Si_{0.01}S_{0.02}$-$MTiO_2$ occurred at the lower pressure. This suggests that $MTiO_2$ has the larger pore size and $Si_{0.01}S_{0.02}$-$MTiO_2$ has the smaller pore size. The narrow pore size distribution curves indicate that the present materials have uniform pore channels. The narrow pore size distribution was not affected by the Si and S codoping.

UV-vis absorption spectra analysis

UV-vis absorption spectra were used to characterize the light absorption ability of the prepared photocatalysts. UV-vis absorption spectra showing the influence of Si and S doping on the UV-vis absorption are given in Fig. 4. Compared with pure $MTiO_2$, there is strong photoabsorption in the visible region (420-700 nm) for the doped $MTiO_2$ photocatalysts and the sample $Si_{0.01}S_{0.02}$-$MTiO_2$ owned the strongest response to visible light. This extended absorbance indicates the possible enhancement in the photocatalytic activity of $MTiO_2$.

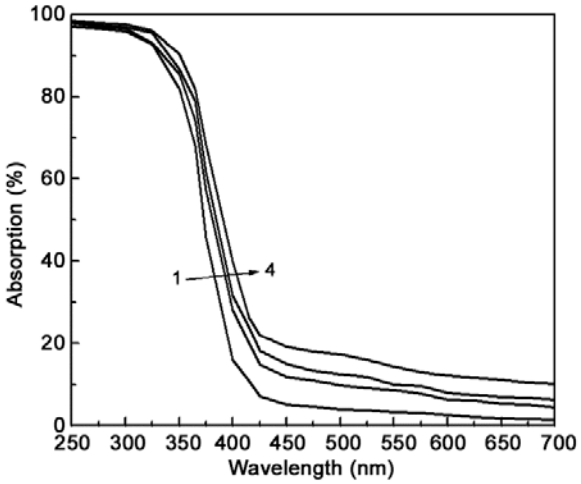

Fig. 4 — UV-vis absorption spectra of $MTiO_2$ and Si-S codoped $MTiO_2$ samples. [$MTiO_2$ (1); $Si_{0.01}$-$MTiO_2$ (2); $S_{0.02}$-$MTiO_2$ (3); $Si_{0.01}S_{0.02}$-$MTiO_2$ (4)].

The red shift of the absorption edge implies decrease in the band gap energy (Eg). The band gap energies of the photocatalysts were calculated (see Table 2) by the formula Eg = 1239.8/λg from the wavelength values corresponding to the intersection point of the vertical and horizontal parts of the spectra (λg).[45] For the pure $MTiO_2$, the Eg is 3.22 eV. In the case of doped $MTiO_2$, Eg decreases from 3.11 to 2.96 eV, while the sample $Si_{0.01}S_{0.02}$-$MTiO_2$ has the lowest band

gap energy (2.98 eV). It is clear that doping led to a modification of the electronic structure around the conduction band edge of $MTiO_2$, thus resulting in the band gap narrowing.

Photocatalytic activity

Photocatalytic activity of Si and S codoped mesoporous TiO_2 was estimated by measuring the degradation rate of MB (20 mg L^{-1}) in the presence of UV and visible light irradiation without considering the degradation intermediates in detail. Pure and single doped mesoporous TiO_2 synthesized by the same method were used as the reference systems. It was found that MB concentration remained stable after 1 h of stirring without illumination in the presence of the obtained samples.

Figure 5 shows the variation of MB degradation with irradiation time under UV light irradiation in the presence of Si and S codoped $MTiO_2$ photocatalysts. It can be observed that all the codoped samples exhibited higher photocatalytic activity than the pure and single doped $MTiO_2$ under UV light irradiation. It can be also seen that the codoped content of the prepared samples had an important effect on the degradation of MB. Among the codoped samples, the best performance was attributed to $Si_{0.01}S_{0.02}$-$MTiO_2$ photocatalyst. The photocatalytic performance of $Si_{0.01}S_{0.02}$-$MTiO_2$ is almost 1.2 times higher than that of pure $MTiO_2$ for degradation of MB under UV light irradiation. This may be due to the positive effect of Si and S on the photocatalytic activity since the codoping not only increases the specific surface area of $MTiO_2$ (see Table 2), but also improves its ultraviolet absorption (see Fig. 4). The specific surface area is one of the key factors to control the photocatalytic activity of a photocatalyst. The larger the specific surface area, the higher is the photocatalytic activity. Furthermore, the photoabsorption character greatly affects the photocatalytic activity of a photocatalyst, since the number of absorbed photons directly depends on the absorption property of the photocatalyst. The photocatalytic activity of Si and S codoped $MTiO_2$ under UV light demonstrates that Si and S codoping effect is outstanding. Such an improvement implies that there is a synergistic effect in the photocatalytic activity when both Si and S are codoped into the $MTiO_2$ photocatalyst.

Figure 6 shows the results of MB degradation with irradiation time under visible light irradiation in the presence of the prepared photocatalysts. It can be seen that all doped samples exhibited photocatalytic activity under visible light. Among the samples, the

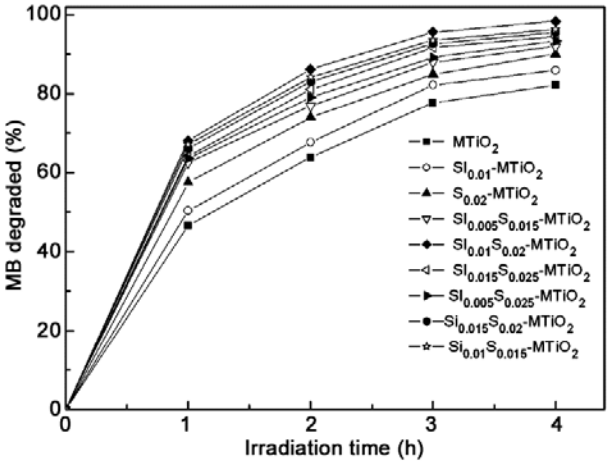

Fig. 5 — Degradation curves of MB with UV light irradiation time.

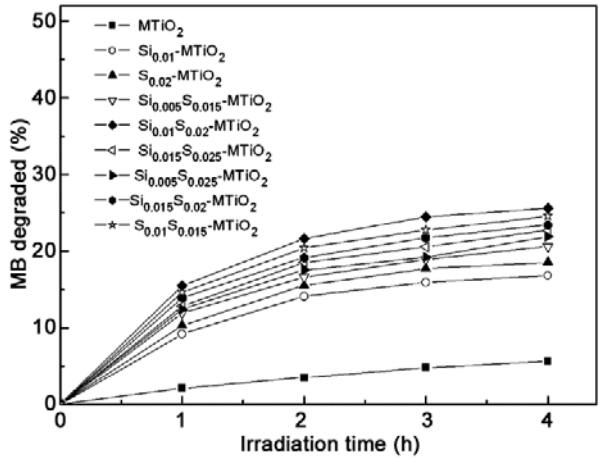

Fig. 6 — Degradation curves of MB with visible light irradiation time.

best performance was attributed to $Si_{0.01}S_{0.02}$-$MTiO_2$, corresponding to the maximum red shift in the UV–vis absorption spectra (see Fig. 4). The photocatalytic performance of $Si_{0.01}S_{0.02}$-$MTiO_2$ was almost twice that of pure $MTiO_2$ for degradation of MB under visible light. From the UV-vis absorption spectra of samples (Fig. 4), it can be seen that the intensity and region of visible light photoabsorption on codoped $MTiO_2$ were stronger and larger than those of pure $MTiO_2$. The strong absorption is beneficial to the photocatalytic activity because the available photons are proportional to photoabsorption. Among the studied samples, $Si_{0.01}S_{0.02}$-$MTiO_2$ showed the best photocatalytic performance. This result is likely to be due to the positive effect of the introduction of Si and S on the photocatalytic activity

because the codoping not only increased the surface area of mesoporous TiO_2 but also extended its photoabsorption to visible light region. According to a previous report,[46] many factors influence the photoactivity of photocatalyst and these factors are closely related to each other. $Si_{0.01}S_{0.02}$-$MTiO_2$ exhibiting the highest photocatalytic activity corresponding to the maximum red shift in the UV-vis absorption spectra (Fig. 4) may be explained by the competition and balance of the above two factors.

Conclusions

A composite photocatalyst of Si and S codoped mesoporous TiO_2 has been successfully prepared by template method using tetraethyl orthosilicate, thiourea and tetrabutyl titanate as precursors and Pluronic P123 as template. The photocatalyst thus prepared was applied for degradation of methyl blue contaminated water. The photocatalyst contained only anatase phase. The Si and S codoping caused the absorption spectra of mesoporous titanium dioxide to shift to the visible region. The doping content had an effect on the photocatalytic activity of the photocatalyst. The synergistic effect of Si and S codoping is responsible for improving the photocatalytic performance. The factors such as surface area, codoping content and photoabsorption affect the photocatalytic activity of Si and S codoped mesoporous titanium dioxide.

Acknowledgment

This work was supported by the National Natural Science Foundation of China (41373127) and the program for Liaoning Excellent Talents in University of China (LR2015052), PR China.

References

1 Phani G, Tulloch G & Vittorio D, *Renewable Energy*, 22 (2001) 303.
2 Kavan L, Rathouský J, Grätzel M, Shklover V & Zukal A, *Microporous Mesoporous Mater*, 44-45 (2001) 653.
3 Young C, Lim T M, Chiang C, Scott J & Amal R, *Appl Catal B*, 78 (2008) 1.
4 Kim S B, Hwang H T & Hong S C, *Chemosphere*, 48 (2002) 437.
5 Jiang D, Zhao H, Zhang S, John R & Will G D, *J Photochem Photobiol A*, 156 (2003) 201.
6 Jiang D, Zhao H, Zhang S & John R, *J Catal*, 223 (2004) 212.
7 Selcuki H, Zaltner W, Sene J J, Bekbolet M & Anderson M A, *J Appl Electrochem*, 34 (2004) 653.
8 Shi Z L, Guo M, Wang L J & Yao S H, *Chinese J Chem Phys*, 29 (2016) 199.
9 Kresge C T, Leonowicz M E, Roth W J, Vartuli J C & Beck J S, *Nature*, 359 (1992) 710.
10 Mitra A, Bhaumik A & Imae T, *J Nanosci Nanotechnol*, 4 (2004) 1052.
11 Liu J, Liu F, Gao K, Wu J S & Xue D F, *J Mater Chem*, 19 (2009) 6073.
12 Das S K, Bhunia M K & Bhaumik A , *Dalton Trans*, 39 (2010) 4382.
13 Xu P, Xu T, Lu J, Gao S, Hosmane N S, Huang B, Dai Y & Wang Y, *Energy Environ Sci*, 3 (2010) 1128.
14 Patra A K, Das S K & Bhaumik A, *J Mater Chem*, 21 (2011)3925.
15 Dutta S, Patra A K, De S, Bhaumik A & Saha B, *ACS Appl Mater Interfaces*, 4 (2012) 1560.
16 Inaba R, Fukahori T, Hamamoto M & Ohno T, *J Mol Catal A*, 260 (2006) 247.
17 Wang Y D, Zhou A N & Yang Z Y, *Mater Lett*, 62 (2008) 1930.
18 Zhang Z, Zuo F & Feng P, *J Mater Chem,* 20 (2010) 2206.
19 Yu J C, Wang X & Fu X, *Chem Mater*, 16 (2004) 1523.
20 Koshitani N, Sakulkhaemaruethai S, Suzuki Y & Yoshikawa S, *Ceramics Int*, 32 (2006) 819.
21 Mao J, Hu X , Li H , Sun Y , C Wang & Z Chen, *Green Chem*, 10 (2008) 827.
22 Yao S H, Zheng Z H, Chen S & Shi Z L, *Chinese J Chem Phys*, 27 (2014) 732.
23 Epifani M , Diaz R, Arbiol J, Comini E , Sergent N, Pagnier T, Siciliano P, Taglia G & Morante J R, *Adv Funct Mat,* 16 (2006) 1488.
24 Long M C, Beranek R, Cai W M & Kisch H, *Electrochim Acta*, 53 (2008) 4621.
25 Pal N, Paul M, Bera A, Basak D & Bhaumik A, *Anal Chim Acta*, 674 (2010) 96.
26 Asahi R, Morikawa T, Ohwaki T, Aoki K & Taga Y, *Science*, 293 (2001) 269.
27 De Vos D E, Dams M, Sels B F & Jacobs P A, *Chem Rev*, 102 (2002) 3615.
28 Martyanov I N, Uma S, Rodrigues S & Klabunde K, *J Chem Commun*, 21 (2004), 2476.
29 Wu J C & Chen C H, *J Photochem Photobiol A*, 163 (2004) 509.
30 Wang C, Böttcher C, Bahnemann D W & Dohrmann J K, *J Nanoparticle Res*, 6 (2004) 119.
31 Xu J, Lu M, Guo X & Li H, *J Mol Catal A*, 226 (2005) 123.
32 Baiju K V, Sibu C P, Rajesh K, Krishna Pillai P, Mukundan P, Warrier K G K & Wunderlich W, *Mater Chem Phys*, 90 (2005) 123.
33 Yao S H, Song S P, Shi Z L, Wang S F, *Desalination & Water Treatment*, 51 (2013) 7101.
34 Shi Z L, Lai H, Yao S H & Wang S F, *Chinese J Chem Phys*, 25 (2012) 96.
35 Lin L, Zheng R Y, Xie J L, Zhu Y X & Xie Y C, *Appl Catal:B*, 76 (2007) 196.
36 Takeshita K, Yamakata A, Ishibashi T A, Onishi H, Nishijima K & Ohnoc T, *J Photochem Photobiol A,* 177 (2006) 269.
37 Li D, Ohashi N, Hishita S, Kolodiazhnyi T & Haneda H, *J Solid State Chem*, 178 (2005) 3293.
38 Zhao W, Ma W H, Chen C C, Zhao J C & Shuai Z G, *J Am Chem Soc*, 126 (2004) 4782.
39 Li Y, Hwang D S, Lee N H & Kim S, *J Chem Phys Lett*, 404 (2005) 25.

40 Li D, Haneda H, Hishita S & Ohashi N *Chem Mater*, 17 (2005) 2588.
41 Sun X, Xing J & Qiu J, *Russ J Phys Chem A*, 90 (2016) 1151.
42 Gregg S J & Sing K S W, *Adsorption, Surface Area and Porosity*, 2nd Edn, (Academic Press, London) 1982.
43 Sing K S W, Everett D H, Haul R A W, Moscou L, Pierotti R A, Rouquerol J & Siemieniewska V T, *Pure Appl Chem*, 57 (1985) 603.
44 Rojas F, Kornhauser I, Felipe C, Esparza J M, Cordero S, Dominguez A & Riccardo J L, *Phys Chem Chem Phys*, 4 (2002) 2346.
45 Yuan R S, Zheng J T, Guan R B & Zhao Y C, *Colloids Surfaces A*, 254 (2005) 131.
46 Li D & Haneda H, *J Photochem Photobiol A,* 160 (2003) 203.